

# Characterisation of thermal stability and phase transformation energetics in tempered 9Cr–1Mo steel using drop and differential scanning calorimetry

S. Raju<sup>a,\*</sup>, B. Jeya Ganesh<sup>a</sup>, Aritra Banerjee<sup>b</sup>, E. Mohandas<sup>a</sup>

<sup>a</sup> Physical Metallurgy Section, Metallurgy and Materials Group, Indira Gandhi Centre for Atomic Research, Kalpakkam 603102, Tamilnadu, India

<sup>b</sup> Department of Physics, University of Kolkata, Kolkata, India

Received 20 July 2006; received in revised form 24 December 2006; accepted 30 January 2007

## Abstract

The thermodynamic stability and phase transformation energetics of a tempered 9Cr–1Mo steel have been studied using drop and isochronal differential scanning calorimetry techniques. The measured enthalpy reveals a steep increase with temperature, especially for temperatures exceeding 650 °C. It is found that the emergence of various phases as a function of temperature has been clearly marked by the presence of distinct inflections in the measured enthalpy increment versus temperature curve, obtained using drop calorimetry. The isochronal differential scanning calorimetry experiments yielded precise values for the transformation arrest points. The ferromagnetic to paramagnetic transformation temperature is found to be about  $740 \pm 5$  °C. The austenite start ( $Ac_1$ ) and finish ( $Ac_3$ ) temperatures recorded during continuous heating are found to be strongly dependent on the heating rate and the extrapolated, so called zero scan rate values are found to be 830 and  $870 \pm 5$  °C, respectively, for  $Ac_1$  and  $Ac_3$ . The process of cooling from austenite field yielded martensite for the cooling rates  $5\text{--}40$  °C  $\text{min}^{-1}$  employed in the present study. The martensite start temperature is fairly independent of the cooling rate and is found to be  $370 \pm 5$  °C. By adopting a phenomenological model for calculating the enthalpy of metastable ferrite at temperatures higher than its known range of stability, the enthalpy change associated with austenitisation ( $\alpha$ -ferrite + carbide  $\rightarrow$   $\gamma$ -austenite) transformation has been estimated as a function of temperature. It is found that in the temperature range 625–1200 °C, the variation of the enthalpy with temperature due to phase change can be considered to be linear, which in effect renders a constant value for the effective transformation specific heat. This value is found to be of the order of  $15.4 \text{ J mol}^{-1} \text{ K}^{-1}$  ( $\pm 8\%$ ) in the temperature interval, 650–1200 °C.

© 2007 Elsevier B.V. All rights reserved.

**Keywords:** Ferritic steel; Enthalpy; Phase transformation; Calorimetry

## 1. Introduction

High chromium ferritic and martensitic steels are among the preferred candidate alloys for making the core structural components of metal-fuelled fast reactors owing to their attractive combination of properties, including adequate swelling resistance against fast neutron irradiation [1–10]. While the literature on the physical metallurgy of ferritic steels is replete with many experimental and modelling studies on the quantitative characterisation of the microstructure that develops during tempering and subsequent long term exposure to simulated operating conditions [11–19], the intrinsic thermodynamic stability of the ferrite matrix itself has not been investigated very extensively. A fundamental investigation on the high temperature thermody-

amic stability of ferritic steel is therefore in order from the point of view of obtaining a balanced and broad-based perspective of the overall thermal stability in this class of materials.

It is in this spirit, that we have undertaken a study on the accurate determination of the temperature variation of the total enthalpy content of a normalised and tempered (N&T) 9Cr–1Mo steel, in the temperature range 22–1200 °C (295–1473 K). The phase changes that are generic to ferritic steels have been clearly finger printed by the presence of distinct non-linear characteristics in the measured enthalpy versus temperature curve. These studies are further supplemented by continuous heating and thermal cycling experiments in a differential scanning calorimeter (DSC) that help in marking precisely the various transformation temperatures as well as the associated transformation kinetics parameters.

Before proceeding further, it is rather useful to recall the basic difference between drop calorimetry and isochronal DSC experiments, as this has a bearing on the correct interpretation of the

\* Corresponding author. Tel.: +91 44 27480 306; fax: +91 44 27480 081.  
E-mail address: sraju@igcar.gov.in (S. Raju).

quantities measured using these two techniques. The former is a static or isothermal experiment performed under more or less full thermal equilibrium of the sample at a fixed preset temperature. It is the differential heat flux between the sample and the hot drop bed that is actually measured in this experiment. This heat flux is converted into relative enthalpy or enthalpy increment using calibration standards. Therefore, measurements of enthalpy at discrete temperature intervals characterise the drop calorimetry experiments. The temperature evolution of enthalpy, being never continuously monitored as a function of temperature, it is not possible to obtain precise values for various transformation arrest points using drop calorimetry. On the other hand, the plausible temperature intervals of phase instability are indicated by the characteristic inflection points in the enthalpy versus temperature curve. The isochronal DSC, on the other hand, is a dynamic technique performed under a constant heating rate. The accuracy of the signal is affected amidst other things by the presence of thermal gradients, thermal lag between the furnace and the actual sample temperature, etc. Nevertheless, by taking proper precautions and ensuring good calibration practices, it is indeed possible to obtain precise estimates of various transformation temperatures using isochronal DSC experiments. The transformation temperatures thus determined are heating rate dependent. It is only by virtue of combining drop and DSC techniques a fairly comprehensive understanding on the phase stability scenario in 9Cr–1Mo steel is attempted in this study.

## 2. Experimental procedure

### 2.1. Sample preparation and preliminary characterisation

The composition of the steel used in the present study is listed in Table 1. The material is supplied in plate form in normalised and tempered condition. The normalisation heat treatment consists of furnace heating the sample to 1050 °C (1323 K) with a holding time of about 15 min at this temperature. This is followed by cooling to room temperature 22 °C (295 K) in air. Optical metallography of the normalised specimen revealed the presence

Table 1  
The composition of 9Cr–1Mo steel used in this study

Element	wt. %
C	0.10
Ni	0.17
Cr	8.44
Mn	0.46
Cu	0.11
Mo	0.94
Si	0.49
P	0.008
S	0.002
V	0.001
Al	0.011
Fe	Balance

The composition analysis has been made using direct reading optical emission spectroscopy. Note that the Cr content is somewhat on the lower side, while nickel is on the higher side as compared to the standard 9Cr–1Mo variety found in literature [10].

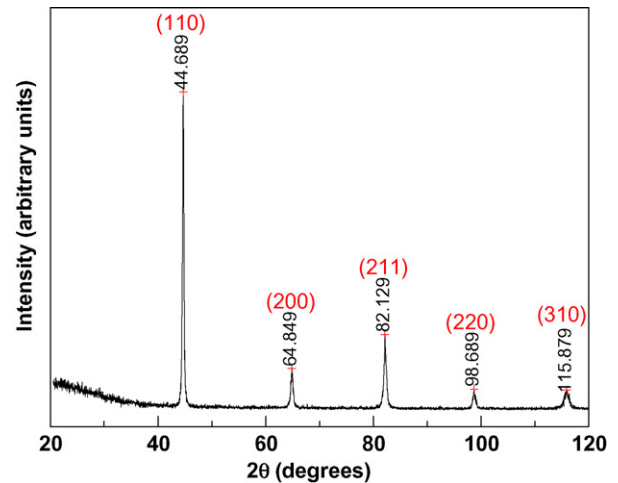


Fig. 1. The room temperature X-ray diffraction pattern of normalised and tempered 9Cr–1Mo steel, taken with Cu K $\alpha$  radiation. Only the presence of ferrite reflections are recorded as the carbide volume fraction is rather small.

of martensitic microstructure. This hard martensite is subsequently tempered by reheating the sample to 780 °C (1053 K) for about 2 h, followed by air cooling to 22 °C (295 K). The average microhardness of the N&T microstructure has been found to be 296 VHN. The room temperature XRD profile is shown in Fig. 1. The mean lattice parameter of the ferrite phase is found to be  $0.2876 \pm 0.003$  nm. This is in fair agreement with the estimated value of 0.2866 nm that is based on the empirical formula suggested by Bhadeshia et al. [20]. The average bulk density of the sample as determined by the standard immersion technique is found to be  $7.67 \times 10^3$  kg m $^{-3}$ . Using this density value and the X-ray lattice parameter of the ferrite phase, the average molecular weight of 9Cr–1Mo ferritic steel is estimated to be  $0.05485$  kg mol $^{-1}$  [21].

### 2.2. Drop calorimetry studies

The drop calorimetry measurements are performed with Setaram-HTC 96<sup>®</sup> high temperature calorimeter. The 9Cr–1Mo samples ( $50\text{--}100 \pm 0.1$  mg) are placed in individual specimen slots, provided with the top assembly of the experimental chamber. In addition, standard samples of  $\alpha\text{-Al}_2\text{O}_3$ , supplied by Setaram are also loaded into the remaining slots of the specimen carousel. The temperatures of the furnace and that of the experimental chamber are independently measured by S-type (Pt–Pt/Rh) thermocouples. The furnace is then gradually ( $10^\circ\text{C min}^{-1}$ ) heated to the desired experimental temperature under argon gas cover. Once the temperature of the alumina bed has reached the pre-set value to within an accuracy of  $\pm 0.1$  K, the samples are dropped from their respective slots through a guiding ceramic tube into the hot alumina bed. The heat absorbed by the specimen upon its drop from ambient temperature into the preheated alumina bed is accurately quantified by monitoring the change in temperature as well as the power supplied to the bed as a function of time. The data acquisition period is dependent on the mass of the sample and in the present set of experiments, a time span of about 20–25 min is followed. Fur-

ther, a gap of about 30 min is maintained between two successive drops. This is necessary for the alumina bed to regain its thermal equilibrium after it has been perturbed by a previous drop experiment. The whole experiment is repeated by dropping  $\alpha\text{-Al}_2\text{O}_3$  standards under identical conditions. Assuming negligible heat loss due to radiation and besides, invoking quasi-adiabatic conditions to prevail in the experimental chamber,  $Q_S(T)$ , the heat energy transported from the bed to the sample may be written as follows [22].

$$Q_S(T) = C(T) \left( \frac{m_S}{M_S} \right) (H_T - H_{22})_S. \quad (1)$$

In Eq. (1),  $m_S$  is the actual mass of the sample,  $M_S$  its molar mass,  $H_T - H_{22}$  is the measured enthalpy increment with respect to  $22^\circ\text{C}$  (295 K), which is the reference temperature and  $C(T)$  is a temperature dependent calorimeter constant. The latter quantity may be obtained from the heat change measured with respect to the standard alumina reference ( $Q_R$ ) and from the knowledge of its critically assessed enthalpy values [23]. Thus,

$$Q_R(T) = C(T) \left( \frac{m_R}{M_R} \right) (H_T - H_{22})_R. \quad (2)$$

In the above expression,  $m_R$  and  $M_R$  denote, respectively, the actual and the molar mass of alumina reference, which is taken to be  $101.96 \times 10^{-3} \text{ kg mol}^{-1}$  [23]. For ferritic steel, the enthalpy values are measured at several temperature intervals in the range  $200\text{--}1200^\circ\text{C}$ . As a matter of ensuring reliability, we also measured the enthalpy of OFHC grade copper (better than 99.99% pure) up to a temperature of  $827^\circ\text{C}$ . An agreement to within  $\pm 5\%$  and up to  $1050^\circ\text{C}$ , is obtained between the values measured using the present equipment and the reported ones [24], including the latest assessment by present authors [25].

### 2.3. Differential scanning calorimetry studies

The DSC studies are performed using Setaram Setsys 16<sup>®</sup> high temperature heat-flux type differential scanning calorimeter. Similar to drop calorimetry experiments, small, well-cleaned samples of mass varying from 40 to 140 mg have been used for DSC experiments. The specimen chamber is alternately evacuated and purged with high pure argon a few times, before the commencement of an experimental run. A steady argon flow of about  $20\text{--}30 \text{ ml min}^{-1}$  is maintained through out the experiment. A typical isochronal DSC run employed in the present study consists of following heating and cooling schedules.

- (i) To begin with, the furnace temperature is gradually raised to  $200^\circ\text{C}$  and is allowed to stabilise at this temperature for about 15 min. This preconditioning facilitates the attainment of a smooth non-wavy baseline. This is followed by the actual heating ramps and holding isotherms characteristic of the present isochronal DSC experiments.
- (ii) In an actual experimental run, the sample is heated at a pre determined rate from  $200$  to  $1000^\circ\text{C}$  or to  $1250^\circ\text{C}$  in some runs and is equilibrated at this temperature for about 15 min, and then cooled at the same scan rate to  $200^\circ\text{C}$ , again kept

at this temperature for a period of about 15 min, before cooling to room temperature. The scanning rate employed varied between  $5$  and  $40^\circ\text{C min}^{-1}$ . The employment of slower scanning rates like  $1^\circ\text{C min}^{-1}$  resulted in some decarburisation of the sample owing to long exposure time. While, fresh samples are employed for each individual run, a few repeat runs were also performed without changing sample. This is carried out with a view to study the effect of thermal cycling on phase transformation behaviour.

- (iii) Base line calibration runs have been performed for each scan rate under identical experimental heating and cooling conditions using the *same* pair of empty crucibles on both sides of the DSC cradle. The temperature calibration has been done using the melting points of pure aluminium, zinc, tin, copper, silver, gold, and Armco iron standards. The heat flow calibration is done in terms of the polymorphic transitions in Armco iron and the melting transition in gold, silver and copper.

## 3. Results

### 3.1. Enthalpy increment versus temperature data

In Fig. 2, the measured enthalpy increment values ( $H_T - H_{22}$ ) for two typical experimental runs are plotted against temperature. Certain salient features are readily apparent from this graph. It is clear that the enthalpy of 9Cr–1Mo steel shows a pronounced increase with temperature and this is in sharp contrast to the rather steady and smooth behaviour witnessed in the case of austenitic stainless steels [26]. The genesis of this basic difference lies in the well-known temperature induced phase instabilities that are typical of a Fe–Cr–Mo–C system [17,27–29]. In the temperature and composition range of our interest, there are in principle three distinct phase transformation stages that mark the phase evolution characteristics of a Cr–Mo low carbon steel possessing quenched martensitic microstructure to start with [17,29,30]. These phase changes may be placed in the following order with respect to increasing temperature [29,30]:

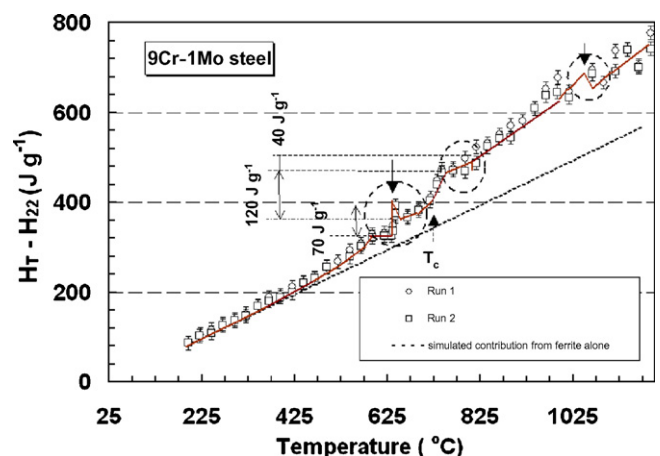


Fig. 2. The temperature variation of enthalpy obtained using drop calorimetry is graphically portrayed.

- (i) Gradual relaxation of martensite over a narrow range of temperature;
- (ii) transformation from ferromagnetic to paramagnetic ferrite;
- (iii) beginning of the formation of austenite as a result of  $\alpha$ -ferrite + carbide  $\rightarrow$  austenite reaction upon crossing the lower critical  $A_{c1}$  temperature, and the notional completion of austenite formation at  $A_{c3}$ , the upper critical temperature;
- (iv) the formation of  $\delta$ -ferrite at higher temperatures.

If the starting microstructure is one of tempered martensite containing carbides mostly of  $M_{23}C_6$  type dispersed in the  $\alpha$ -ferrite matrix, then the  $\alpha$ -ferrite + carbide  $\rightarrow$  austenite transformation is the major reaction taking place upon continuous heating. The magnetic transformation is of course still present, but is rather comparatively weak from the energetics point of view.

It must be mentioned that if initial tempering was not properly carried out in the sense, that the starting microstructure contained some traces of untempered martensite, then it follows during heating that this untempered martensite fraction might start precipitating carbides upon reaching appropriate temperature. It must also be noted that this decomposition step is initiated at temperatures less than  $A_{c1}$ , which marks the beginning of austenite formation during continuous heating. In other words, the small scale tempering reaction might occur along with the austenitisation of the major  $\alpha$ -ferrite + carbide phase. It is worth noting that in general the diffusional decomposition of tempered martensite entails a measurable change in the total enthalpy content, primarily because of a change in composition and the phase fraction of the corresponding microstructural constituents [29,30]. The drop calorimetry measurements as mentioned in the previous section follow the enthalpy effects that are associated with isothermal anneals performed at discrete temperature intervals. Therefore, an appreciable or step like change in enthalpy as reflected in Fig. 2 is a tell-tale signature of the phase evolution characteristics, although the precise fixation of the transformation temperature domain is not facilitated by drop calorimetry measurements.

In Fig. 2, the approximate domains of occurrence of diverse phase transformations are indicated by dotted envelopes. As may be seen, the first one is a fairly sharp peak positioned around  $640 \pm 5^\circ\text{C}$  (915 K) and is accompanied by a measurable enthalpy change. This could arise from the beginning of the decomposition of untempered martensite if any present. It may be noted that a temperature of about  $640^\circ\text{C}$  or so is adequate to initiate this reaction as there could be an appreciable mobility of interstitial carbon as well as some grain boundary diffusion of chromium atoms at this temperature [31]. Further, it is also observed from Fig. 2 that this transformation is featured by an enthalpy change of about  $70 \pm 8 \text{ J g}^{-1}$ , which translates to  $3.84 \text{ kJ mol}^{-1}$  for the present steel. It is also instructive to note that the enthalpy curve continues to rise rather steeply subsequent to this event, which implies that the phase evolution has just begun and in fact is still vibrantly taking place in the sample. Stating in quantitative terms, a steep enthalpy increase of about,  $120 \pm 8 \text{ J g}^{-1}$  is estimated for a change in temperature of about  $80^\circ\text{C}$  in the temperature range  $650\text{--}730^\circ\text{C}$

(Fig. 2). This increase derives both from the change in heat capacity of the system brought upon by the ferromagnetic to paramagnetic transition, in addition to the beginning of the compositional and phase fraction modification of ferrite and carbide mixture. It emerges from literature that the Curie point for standard 9Cr–1Mo composition lies around  $740 \pm 5^\circ\text{C}$ ; for pure iron it is at  $770^\circ\text{C}$  [32]. But a clear attestation of the magnetic transformation is somewhat masked in the present study by the closely attending austenite formation reaction.

The second phase instability domain starts from  $747^\circ\text{C}$  in the form of a steady continuing rise in enthalpy that persists right up to  $1050^\circ\text{C}$ . These temperatures are only suggestive of the probable domain, since as mentioned before, no continuous monitoring of phase evolution is possible in drop calorimetry studies. This increasing region in enthalpy marks the beginning and probably the near culmination of the austenite formation from  $\alpha$ -ferrite + carbides, respectively.

Another distinct step or for that matter a sharp arrest point in the enthalpy curve is noticed at around  $1020 \pm 5^\circ\text{C}$  (Fig. 2). According to an early report by Sanderson [18], the computed constant carbon section of (Fe– $x$ Cr–0.1 wt.%C) system suggests that for a steel of about 9 wt.% Cr, the  $\delta$ -ferrite phase begins to appear around  $1100^\circ\text{C}$ . Also a recent study on Eurofer 97 (another nuclear grade ferritic steel that is closely related to 9Cr–1Mo variety) a temperature of about  $1200^\circ\text{C}$  (estimated using Thermo Calc software) marks the arrival of the  $\delta$ -ferrite phase on cooling from liquid [33]. Taking into account the slight differences in composition between 9Cr–1Mo and Eurofer 97, and also bearing in mind the possible discrepancy between the calculated and experimental transformation arrest points and also the role of hysteresis between cooling and heating cycles, the inflection at  $1050^\circ\text{C}$  witnessed in the present isothermal drop calorimetry measurements for standard 9Cr–1Mo steel, can be taken to mark the entry of the system into the  $\gamma$  +  $\delta$ -ferrite two phase field on continuous heating. On the other hand, the dilatometry study of Garcia de Andres et al. on low carbon–low alloy steels [34] suggests that although the austenite formation is supposed to be complete upon crossing  $A_{c3}$ , it requires some superheating in the case of rapid continuous heating experiments to even out the composition fluctuations and to attain what is known as the homogeneous austenite phase. Combining these two possibilities, it is believed that the inflection in enthalpy seen at  $1020^\circ\text{C}$  (Fig. 2) is associated with both austenite homogenisation and the possible emergence of  $\delta$ -ferrite from homogeneous austenite. Detailed metallography on high temperature quenched samples is underway to shed further light in this regard.

As a passing remark, it must be reiterated that in drop calorimetry measurements, no matter how close the temperature interval between successive experimental points are selected, it is virtually impossible for obvious reasons to trace the evolution of various phases in a truly continuous manner. Despite the fact that quite a good number of repeat runs are performed near the suspected transformation onsets and finish temperatures, primarily to ensure reproducibility as well as to enhance the statistical weight of the observed transformational enthalpy changes, varying extent of transformations especially in samples of different masses prevented from getting a better than 8% accuracy for the

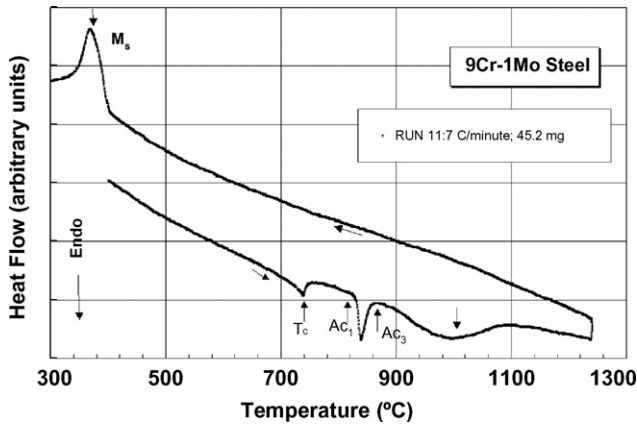


Fig. 3. A typical DSC trace obtained during heating and cooling schedule. The arrow at  $T_C$ , marks the magnetic transformation point, while at  $Ac_1$  and  $Ac_3$  denote, respectively, the austenite start and end temperatures.  $M_S$  indicates the martensite start temperature during cooling.

transformation enthalpy changes. The calibration of uncertainty in this case is made by recording the enthalpy changes associated with the polymorphic transitions of Armco iron [33]. A precise determination of transformation arrest points from the observed inflection points in the enthalpy versus temperature curve also suffered due to this reason. Towards the cause of estimating precisely the various transformation points, continuous heating experiments in DSC have been performed. These results are presented below.

### 3.2. DSC data: continuous heating thermograms

In Fig. 3, a typical DSC thermogram obtained in the process of heating and cooling schedule is shown. The presence of two distinct endothermic peaks marked as  $T_C$  and  $Ac_1$ – $Ac_3$  in the figure, delineate the stability domain of (non-magnetic) ferrite and that of austenite+ferrite phase field. In particular, the temperature space enclosed between  $Ac_1$  (austenite onset temperature)– $Ac_3$  (austenite finish temperature) characterises the ferrite + austenite + carbide (undissolved) three-phase region. The peak corresponding to  $T_C$  is somewhat diffuse, as compared to the austenite formation reaction peak at  $Ac_1$ – $Ac_3$ . After  $Ac_3$ , the sample is mostly austenitic, although the complete homogenisation of it may not yet been realised at this stage [34]. This is attested by the presence of a rather broad endothermic trough after  $Ac_3$ , the peak position of which seen at  $1020 \pm 5^\circ\text{C}$ . This may mark the plausible evolution of homogeneous austenite, or as discussed in the previous section, it might also herald the concurrent emergence of  $\delta$ -ferrite [33]. On the cooling cycle, the diffusional decomposition of austenite is fully suppressed, resulting in the formation of martensite upon reaching  $M_S$  [18].

The heating and cooling rate sensitivity of various transformation points ( $T_C$ ,  $Ac_1$  and  $Ac_3$ ) has been studied by employing a range of scan rates varying from 5 to  $40^\circ\text{C min}^{-1}$ . The typical results are portrayed in Fig. 4. As may be seen, the transformation temperatures shift to higher values with increasing scan rate in the heating cycle, while the reverse is true for the  $M_S$

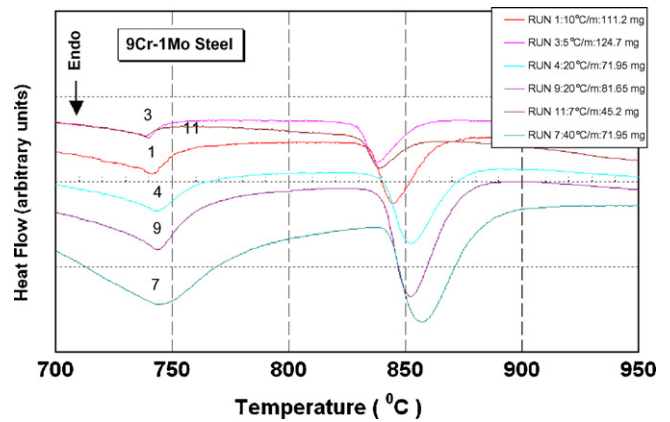


Fig. 4. DSC traces obtained with different sample masses and at different heating rates. Note that the y-axis, representing the differential heat flow is arbitrarily scaled in order to accommodate different traces in a single graph.

temperature during the cooling cycle (not shown in Fig. 4). It may further be noted that the cooling rate sensitivity of  $M_S$  is only marginal. A graphical depiction of the scan rate sensitivity of the transformation temperatures is presented in Fig. 5. In this figure,  $Ac^*$  corresponds to the peak temperature of the ferrite + carbide  $\rightarrow$  austenite transformation reaction. That is  $Ac_1 < Ac^* < Ac_3$ . The extrapolated zero scan rate value of  $T_C$  is found to be  $738^\circ\text{C}$ . Although the temperature spread between  $Ac_1$  and  $Ac_3$  is found to be a strong function of heating rate and sample mass, the peak temperature  $Ac^*$  revealed a linear scaling with the heating rate (Fig. 5) and a value of about  $836^\circ\text{C}$  is obtained for the hypothetical zero scan rate. This temperature compares well with the dilatometry based results for Eurofer 97 [33]. Moreover, for a typical heating rate of about  $20^\circ\text{C min}^{-1}$ , the  $Ac_1$  and  $Ac_3$  are estimated to be about  $830$  and  $870 \pm 5^\circ\text{C}$ , respectively, for a sample mass of  $70\text{ mg}$ .

It must be added that we did not perform experiments at very slow heating rates ( $\leq 1^\circ\text{C min}^{-1}$ ) since some specimen decarburisation is observed at longer times. It may be stated that the present values of  $Ac_1$  and  $Ac_3$  represent the upper

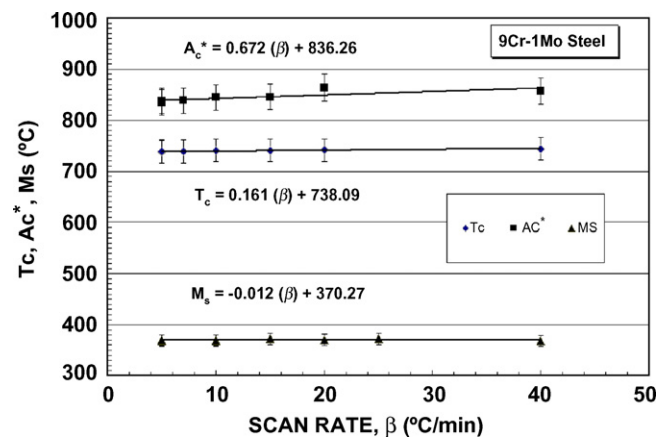


Fig. 5. The scan rate sensitivity of various transformation peaks seen in DSC is graphically portrayed.  $Ac^*$  denotes the peak temperature for  $\alpha$ -ferrite + carbide  $\rightarrow$  austenite transformation.

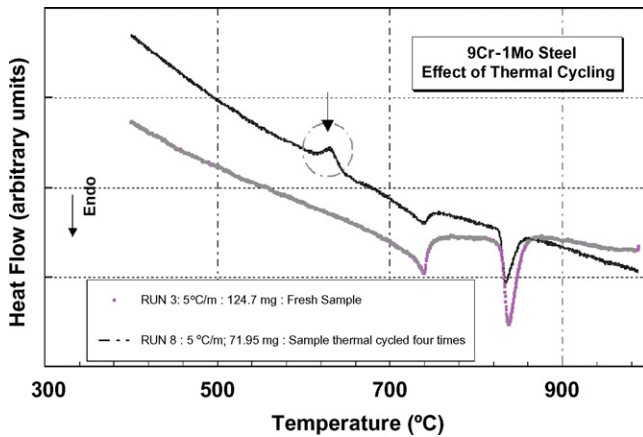


Fig. 6. Effect of thermal cycling in DSC is illustrated. Note the appearance of a new peak in the thermally cycled sample at about 623 °C.

bound estimates of the corresponding equilibrium transformation temperatures  $A_1$  and  $A_3$  that may possibly be obtained if the experiments were performed under infinitely small heating rates. In a similar manner, the zero scan rate  $M_S$  temperature is estimated to be  $370 \pm 5$  °C. It must be added that the  $M_S$  temperature obtained in the present study exhibits a remarkable agreement with the value of 370.5 °C, estimated using Andrew's empirical formula [35]

$$M_S(^{\circ}\text{C}) = 539 - 423 \text{ wt.\% C} - 30.4 \text{ wt.\% Mn} - 17.7 \text{ wt.\% Ni} \\ - 12.1 \text{ wt.\% Cr} - 7.5 \text{ wt.\% Mo.} \quad (3)$$

However, the application of the formula based on artificial neural network model [36] resulted in a slightly higher value of 397.5 °C. In the latter case, the  $M_S$  temperature is estimated using the following expression

$$M_S(^{\circ}\text{C}) = 764.2 - 30.2 \text{ wt.\% C} - 30.6 \text{ wt.\% Mn} - 16.6 \text{ wt.\% Ni} \\ - 8.9 \text{ wt.\% Cr} + 2.4 \text{ wt.\% Mo} - 11.3 \text{ wt.\% Cu} \\ + 8.5 \text{ wt.\% Co} + 7.4 \text{ wt.\% W} - 14.5 \text{ wt.\% Si.} \quad (4)$$

### 3.3. Effect of thermal cycling

While continuous heating DSC runs performed with fresh samples revealed peaks corresponding only to reactions at  $T_C$  and  $Ac_1$  and  $Ac_3$ , an interesting feature is noted, when samples are thermal cycled in DSC under argon atmosphere. This thermal cycling treatment consists of heating the sample to 1250 °C (austenite +  $\delta$ -ferrite field) with a hold of about 15 min at this temperature, followed by cooling at a predetermined rate to room temperature. This heating and cooling cycles are repeated a few times. In one such experiment, the DSC trace during the heating cycle of a sample that has been previously cycled four times, revealed a clear exothermic peak at about 623 °C. This is illustrated in Fig. 6. While, a mild exothermic trough has started appearing even during the first course of recycling, this developed into a sharply resolved peak only upon repeated cyclic heat treatments. A reference to literature on general phase stability of 9Cr–1Mo based ferritic steels suggests that a prolonged

hold at 1250 °C is adequate to dissolve all the carbides yielding thereby a stable austenite bay, which upon cooling gives rise to martensitic microstructure at room temperature. It is the heat effects associated with the tempering of the quenched martensite giving rise to  $\alpha$ -ferrite + carbide that is responsible for the exothermic peak at 625 °C. It is added that the peak temperature of this precipitation event has been found to be a function of scan rate.

## 4. Discussion

### 4.1. Transformation energetics

At the outset, it is useful to recall the fact that phase evolution in ferritic steel during continuous heating is one of strongly non-equilibrium in character [29,30,37]. Given sufficiently longer times, the phases observed at any particular isothermal temperature hold may be somewhat different at least in composition, from the ones that are witnessed within the limiting time span of our drop calorimetry experiments.

The phase evolution in ferritic steels is one of involving a dynamical interplay between nucleation, growth and coarsening of various metastable and stable phases [12]. Just as in the case of Fe–C binary, not only the phase fraction of the emerging constituents undergo a continual change, their compositions too exhibit concurrent modification [37]. At present, these issues concerned with thermodynamic and kinetic aspects of phase transformations in steels are tackled by phenomenological approaches [38], a gainful application of which requires precise knowledge of the thermodynamic driving forces behind various precipitation reactions. In this regard, to the best of our knowledge, we are not aware of any previous calorimetry based studies on this steel performed with a view to elicit the thermodynamic quantities connected with phase transformation energetics. The experimental calorimetry data obtained in this study will certainly be a useful supplement to the existing state of knowledge on issues related to thermodynamic modelling of phase transformations in ferritic steels.

The drop calorimetry measurements performed under near thermal equilibrium conditions (not thermodynamic equilibrium; but thermal gradients within the sample are appreciably absent) give reliable estimates of the total enthalpy changes as a function of temperature. The approximate regimes of phase transformation are attested by distinct changes in the slope of the enthalpy versus temperature curve (Fig. 2). It must be remarked that contrary to the case of a phase change in pure unary systems, the estimation of transformation enthalpies is not a straightforward task in systems like ferritic steels experiencing continuous phase evolution. This is because of the fact that not the entire quantum of the measured jump in enthalpy at the transformation point comes from the so-called latent heat of phase change. In fact, a sizeable fraction of the observed heat change derives from the enthalpy that is required to heat the untransformed fraction of the ferrite plus carbide mixture to the concerned equilibrium temperature [37]. This heat, albeit small at lower end of the transformation temperature domain, becomes substantial as temperature goes up. This contribution must therefore be sub-

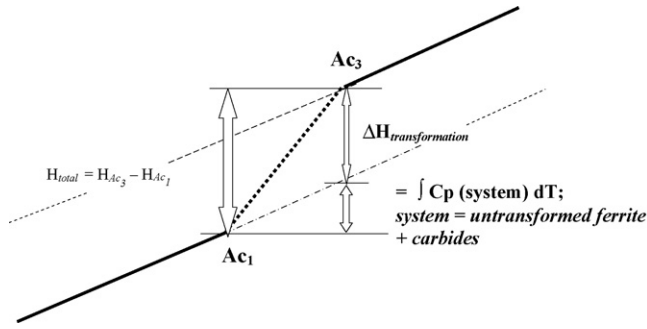


Fig. 7. The methodology adopted for estimating the contribution to enthalpy coming from a phase change is illustrated.

tracted from the measured total change in enthalpy in order to obtain the true quantum of latent heat of phase transformation. This point is graphically explained in Fig. 7.

In Fig. 7, the measured difference in enthalpy between the two nodal points of ferrite → austenite formation, namely  $Ac_3$  and  $Ac_1$ , is split into two additive contributions. That is,

$$H_{Ac_3} - H_{Ac_1} = \int C_p(\text{system}) dT + \Delta H_{\text{transformation}} \quad (5)$$

where system = untransformed ferrite + carbide; and

$$\Delta H_{\text{transformation}}(Ac_3) = H_{\text{austenite+carbide}} - H_{\text{ferrite+carbide}} \quad (6)$$

It is clear that just before  $Ac_1$ , the system is constituted of the two-phase mixture ferrite + carbides; between  $Ac_1$  and  $Ac_3$ , it is a mixture of ferrite, carbide and austenite. Further, it is obvious that between  $Ac_1$  and  $Ac_3$ , the phase fraction of austenite (ferrite) is increasing (decreasing) with temperature. Now, let us consider a hypothetical process, in which, we do not allow the ferrite fraction at  $Ac_1$  to decompose, but instead superheat the system en masse to  $Ac_3$ . The change in enthalpy of the system (ferrite + carbide) in this case is traced by the extrapolated dotted line emanating from the reference temperature  $Ac_1$ . The total enthalpy change for this step is given by  $\int C_p(\text{system}) dT$ ; and this contribution is marked by the short vertical arrow in Fig. 7. At  $Ac_3$ , the superheated ferrite + carbide mixture is allowed to transform to produce austenite. This athermal component of enthalpy, which is characteristic of the latent heat of phase change, is marked by the long vertical arrow in Fig. 7. It is clear from this scheme that between  $Ac_1$  and  $Ac_3$ ,  $\Delta H_{\text{transformation}}$  varies from zero to a maximum. In Fig. 7, for simplicity, the enthalpy change between  $Ac_1$  and  $Ac_3$  is taken to be linear in temperature suggesting that  $\Delta C_p$  due to phase transformation is a constant quantity. But in reality, this need not be so, and a non-linear term is needed for accurately portraying the temperature variation of transformation specific heat.

In the light of the framework discussed above, we need a methodology to extrapolate the enthalpy of ferrite + carbide mixture to higher temperatures, at the least up to  $Ac_3$  to obtain the enthalpy contribution that is due only to austenite formation. The temperature  $Ac_3$  is suggested only as an upper limit of ferrite stability on a notional basis, knowing fully well that  $Ac_3$  is actually dependent on heating rate and thermal history. An approximate method for estimating the enthalpy of metastable

ferrite is suggested here. In what follows, a simple Debye like scheme for extrapolating the enthalpy of ferrite to higher than its stability domain is adopted. The presence of carbide is ignored for computational felicity. Since the volume fraction of the carbide phase is rather small, it is believed that this approximation does not alter the qualitative nature of the conclusions arrived at in this study.

#### 4.2. Extrapolation of the enthalpy of ferrite to higher temperatures

The enthalpy increment is given by the standard thermodynamic expression,

$$\Delta H = \Delta U + p\Delta V \quad (7)$$

In Eq. (7),  $\Delta U$  is the internal energy contribution and  $p\Delta V$  is the contribution from isobaric thermal expansion. Following our earlier research on the thermal property simulation of austenitic steels, the temperature dependent  $\Delta U$  is approximated by Nernst-Lindemann energy function [39].

$$U = \left(\frac{3}{4}\right) n R \theta \left\{ \left[ \frac{2}{e^{\theta/T} - 1} + \frac{1}{e^{\theta/2T} - 1} \right] \right\} \quad (8)$$

This function is an effective hybrid of Debye and Einstein models for polyatomic solids. In the above expression,  $n$  is the number atoms in the unit cell of ferrite, for bcc it is taken as 2,  $R$  the universal gas constant, and  $\theta \approx 0.77\theta_D$  is an empirically scaled Debye temperature of the ferrite phase [39]. Since reliable low-temperature specific heat data are not readily available for the material under study, the following approximation for scaling  $\theta_D$  among isostructural compounds is used [40]

$$\theta_D = \text{Constant} \times \left( \frac{M_{\text{av}}}{\rho_{\text{av}}} \right)^{1/2} \quad (9)$$

For reference, we take the  $\theta_D = 464$  K, of pure  $\alpha$ -iron with a density value of  $7.874 \times 10^3 \text{ kg m}^{-3}$ . The  $\theta_D$  thus estimated turns out to be 458 K. In the next step, the second term in Eq. (7), namely the dilatational correction is estimated by adopting Wachtman's model of thermal expansion [41]

$$\frac{V}{V_0} = \left\{ \frac{U}{Q_0 - kU} + 1 \right\} \quad (10)$$

where  $V/V_0$  is the ratio of the molar volume at a chosen temperature to that at reference temperature, which is taken here as the room temperature.  $Q_0 = (C_p/\alpha_v)_0$  is the ratio of specific heat to volume thermal expansivity at the reference temperature. From literature data,  $Q_0$  is estimated to be of the order of  $1.6 \times 10^7 \text{ J kg}^{-1}$  [39].  $k$  is a material dependent parameter, whose value is given in terms of the pressure derivative of bulk modulus, and its value for 9Cr–1Mo steel is estimated to be 0.8 [39]. Thus, using Eqs. (7)–(10), a theoretical estimate of enthalpy increment of pure ferrite as a function of temperature has been arrived at. These estimated values are shown in Fig. 2 by the thick dotted line. It is instructive to note that up to a temperature of about  $450^\circ\text{C}$ , there is reasonable agreement between the ferrite alone contribution and the measured experimental

enthalpy values. This suggests that any deviation thereof at high temperatures must come from the dynamically evolving phase constitution, namely the changing volume fraction as well as composition of ferrite + carbide + austenite.

Now, looking at Fig. 2, if an estimate of the phase transformation enthalpy with respect to a new reference phase temperature other than 200 °C is desired, it is clear that this hypothetical pure ferrite contribution must be reevaluated with respect to the new reference point. The reason for this is as follows. Although the effect of phase instability of the ferrite matrix has started manifesting from 450 °C itself, the first prominent sign of phase change is found near 625–650 °C. Therefore, it is decided to set this as the reference temperature for the purpose of evaluating the enthalpy arising from phase transformation. At 650 °C, the composition of ferrite is different from that at lower temperatures, which results in different density and hence Debye temperature. To incorporate these factors in a realistic way in the present modelling scheme is a tall order. Instead, what is done is that a parallel to the dotted line depicting the hypothetical pure ferrite contribution with respect to 200 °C is drawn at 650 °C. This is also shown as another thin dotted line in Fig. 2, and this serves as the much needed enthalpy curve of pure ferrite for  $650 \leq T \leq A_{c3}$ . Having thus established all the required inputs, the phase change enthalpy can now be estimated as a function of temperature, using the construct outlined in Fig. 7. That is,

$$\begin{aligned} \Delta H_{\text{transformation}} &= (H_T - H_{650}) - (H_{T^*} - H_{650}) \\ &= H_T - H_{T^*} \end{aligned} \quad (11)$$

$H_{T^*}$  is the enthalpy at temperature  $T$  measured on the hypothetical, extrapolated pure ferrite curve. The ‘\*’ sign stands for the fact that the concerned enthalpy increment is with respect to a fictitious reference state.

The transformation enthalpy thus estimated is plotted as a function of temperature in Fig. 8. As can be seen,  $\Delta H_{\text{transformation}}$  increases steadily with temperature and reaches a plateau at about 1050 °C, at which temperature the formation of homogeneous austenite may start taking place. The curve is not smooth for obvious reasons, since the course of increasing temperature

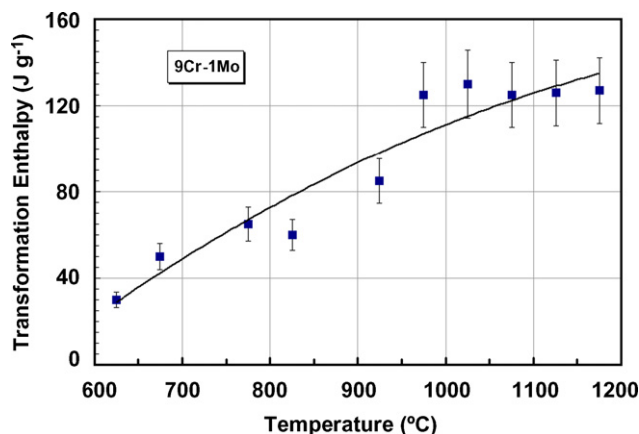


Fig. 8. The temperature variation of transformation enthalpy obtained in the present study is graphically portrayed.

is punctuated by the onset of various phase transformations. At transformation arrest points, there will be inflections in the estimated  $\Delta H_{\text{transformation}}$  versus temperature curve. But this is not that clearly seen in the Fig. 8. This is due to rather high ( $\pm 12\%$ ) experimental uncertainty in the estimated  $\Delta H_{\text{transformation}}$  values in the present study. A considerable portion of this uncertainty is due to the intrinsic scatter associated with the measured enthalpy values at high temperatures. The measured transformation enthalpy values are fitted to the following polynomial in the temperature increment

$$\begin{aligned} \Delta H_{\text{transformation}} (\text{J g}^{-1}) &= 28.805 + 0.2774(T - 625) \\ &\quad - 0.0002(T - 625)^2. \end{aligned} \quad (12)$$

This expression is valid for temperatures exceeding 625 °C. The magnitude of the quadratic term being small that it may be ignored for all practical purposes. This gives a constant value of  $\sim 0.28 \text{ J g}^{-1} \text{ K}^{-1}$  ( $15.358 \text{ J mol}^{-1} \text{ K}^{-1}$ ) for the  $\alpha$ -ferrite + carbide  $\rightarrow$  austenite transformation specific heat. Although no specific data may be gathered from literature with respect to transformation thermodynamics and associated parameters on 9Cr–1Mo steel, the value of about  $15.4 \text{ J mol}^{-1} \text{ K}^{-1}$  for the transformation specific heat is of the same order as that found in low carbon alloy steels [37]. As a final point, it may also be remarked that in arriving at this estimate, no a priori information on the extent of transformation as a function of temperature is assumed, as for example done in the case of an analysis of DSC results in terms of Johnson-Mehl-Avrami plots [37]. In fact, a combined analysis of drop calorimetry based integral transformation enthalpy data in the light of a standard model on transformation kinetics as suggested by DSC result will yield a more comprehensive picture of phase stability and phase transformation scenario in ferritic steels [33]. Further work in this direction is currently underway.

## 5. Conclusions

A comprehensive characterisation of the thermodynamic stability of tempered 9Cr–1Mo steel has been performed using drop and differential scanning calorimetry techniques. The drop calorimetry based total enthalpy measurements clearly attested to the sequence of various phase changes that occur in tempered ferritic steel as a function of temperature. An analysis of these data in terms of a simple phenomenological construct yielded reliable values for the overall transformation enthalpy. A precise determination of various transformation temperatures during continuous heating, namely  $T_C$ ,  $A_{c1}$ ,  $A_{c3}$  and  $M_S$  is made using continuous heating and cooling experiments in DSC.

## Acknowledgements

The authors gratefully acknowledge the sustained encouragement and support provided by Dr. Baldev Raj, Dr. P.R. Vasudeva Rao and Dr. M. Vijayalakshmi. The samples used in this study are courtesy of Dr. Vibhor Chaswal.

## References

- [1] W.L. Bell, T. Lauritzen, S. Vaidyanathan, in: J.W. Davis, D.J. Michel (Eds.), *Topical Conference on Ferritic Alloys for Use in Nuclear Energy Technologies*, ASM, Met. Soc. of AIME, Warrendale, PA, 1983, pp. 113–124.
- [2] J.W. Davis, *J. Nucl. Mater.* 122/123 (1984) 3.
- [3] J. Orr, S.J. Sanderson, in: J.W. Davis, D.J. Michel (Eds.), *Topical Conference on Ferritic Alloys for Use in Nuclear Technologies*, Met. Soc. of AIME, Warrendale, PA, 1984, pp. 261–267.
- [4] T. Fujita, *ISIJ Int.* 32 (1992) 175.
- [5] R.L. Klueh, K. Ehrlich, F. Abe, *J. Nucl. Mater.* 191–194 (1992) 116.
- [6] M. Tokiwai, M. Horie, K. Kako, M. Fujiwara, *J. Nucl. Mater.* 204 (1993) 56.
- [7] M. Tamura, H. Hayakawa, M. Tamimura, A. Hishinuma, T. Kondo, *J. Nucl. Mater.* 155–157 (1988) 620.
- [8] B. Van der Schaaf, D.S. Gelles, S. Jitsukawa, A. Kimura, R.L. Klueh, A. Moslang, G.R. Odette, *J. Nucl. Mater.* 283–287 (2000) 52.
- [9] S. Ukai, M. Harada, H. Okada, M. Inoue, S. Nomura, S. Shikakura, K. Asabe, T. Nishida, M. Fujiwara, *J. Nucl. Mater.* 204 (1993) 65.
- [10] R.L. Klueh, *Int. Mater. Rev.* 50 (2005) 287.
- [11] J.M. Vitek, R.L. Klueh, *Metall. Trans.* 14A (1983) 1047.
- [12] J. Hald, L. Korcakova, *ISIJ Int.* 43 (2003) 420.
- [13] M. Taneike, K. Sawada, F. Abe, *Metall. Trans.* 35A (2004) 1255.
- [14] N. Fujita, H.K.D.H. Bhadeshia, *ISIJ Int.* 42 (2002) 760.
- [15] A. Bjarbo, M. Hallestrand, *Mater. Trans.* 32A (2001) 19.
- [16] A. Kumar, K. Laha, T. Jayakumar, K.B.S. Rao, B. Raj, *Mater. Trans.* 33A (2002) 1617.
- [17] A. Kroupa, J. Havrankova, M. Koufalova, M. Svoboda, J. Vrestal, *J. Phase Equilib.* 22 (2001) 312.
- [18] S.J. Sanderson, *Ferritic Steels for Fast Reactor Steam Generators*, BNES, London, 1978, p. 120.
- [19] B. Nath, E. Metcalfe, J. Hald, in: A. Strang, D.J. Gooch (Eds.), *Microstructural Development and Stability in High Chromium Ferritic Steels*, The Inst. of Materials, London, 1997, p. 123.
- [20] H.K.D.H. Bhadeshia, S.A. David, J.M. Vitek, R.W. Reed, *Mater. Sci. Technol.* 7 (1991) 686.
- [21] A. Jablonska, K. Harste, K. Schwerdtfeger, *Steel Res.* 62 (1991) 24.
- [22] J. Leitner, A. Strejc, D. Sedimudubsky, K. Ruzicka, *Thermochim. Acta* 401 (2003) 169.
- [23] D.G. Archer, *J. Phys. Chem. Ref. Data* 22 (1993) 1441.
- [24] V.Ya. Chekhovskoi, Y.V. Gusev, V.D. Tarasov, *High Temp. High Press.* 34 (2002) 291.
- [25] S. Raju, K. Sivasubramanian, E. Mohandas, *Solid State Commun.* 124 (2002) 151.
- [26] A. Banerjee, S. Raju, R. Divakar, E. Mohandas, G. Panneerselvam, M.P. Antony, *J. Nucl. Mater.* 347 (2005) 20.
- [27] C. Qiu, *Steel Res.* 64 (1993) 618.
- [28] J. Sopousek, J. Vrestal, *Zeits. Metallk.* 85 (1994) 116.
- [29] M. Van Rooyen, E.J. Mittemeijer, *Scr. Metall.* 16 (1982) 1255.
- [30] E.J. Mittemeijer, F.C. Van Doorn, *Metall. Trans.* 14A (1983) 976.
- [31] Zs. Tokei, K. Hennessen, H. Viefhaus, H.J. Grabke, *Mater. Sci. Technol.* 16 (2000) 1129.
- [32] R.K. Williams, R.S. Graves, F.J. Weaver, D.L. McElroy, *Proceedings of 17th International Thermal Conductivity Conference*, Gaithersburg, 1981.
- [33] A. Danan, C. Servant, A. Alamo, J.C. Brachet, *Mater. Sci. Eng. A* 348 (2003) 122.
- [34] C. Garcia de Andres, F.G. Caballero, C. Capdevila, L.F. Alvarez, *Mater. Char.* 48 (2002) 101.
- [35] K.W. Andrews, *J. Iron Steel Inst.* 203 (1965) 721.
- [36] C. Capdevila, F.G. Caballero, C. Garcia de Andres, *ISIJ Int.* 42 (2002) 894.
- [37] G.P. Krielaart, C.M. Brakman, S. Van der Zwaag, *J. Mater. Sci.* 31 (1996) 1501.
- [38] A. Schneider, G.I. Inden, *Acta Mater.* 53 (2005) 519.
- [39] R. Jose, S. Raju, R. Divakar, E. Mohandas, G. Panneerselvam, M.P. Antony, K. Sivasubramanian, *J. Nucl. Mater.* 317 (2003) 54.
- [40] E.F. Steigmeier, *Appl. Phys. Lett.* 3 (1963) 6.
- [41] J.B. Wachtman, T.G. Scuderi, G.W. Gleek, *J. Am. Ceram. Soc.* 45 (1962) 310.